Chapter 2

A survey of waves in random media

Summary

This chapter provides an introduction in the theory of wave propagation and scattering in random media needed for the further understanding of subsequent chapters. The literature on this topic is quite extensive. More detailed information can be found in the review articles of Tourin et al. (2000), Papanicolaou (1998), Frisch (1968), Keller (1960, 1964), and in the classical textbooks of Rytov et al. (1989), Ishimaru (1978), and Chernov (1960). Treatments of scattering phenomena in seismology are provided in Aki and Richards (1980) and Sato and Fehler (1998). All discussed aspects involve statistical methods. The necessary background can be found in Papoulis (1984), Gardiner (1990) and Hohnerkamp (1990). Apart from theoretical considerations, we present a numerical strategy to simulate wave propagation in 2-D and 3-D random media. Properties of scattered wave fields are numerically analyzed.

In section (2.1) we present a brief outline of multiple scattering theories based on stochastic wave equations and their ranges of applicability. We focus on methods developed for weak and strong scattering, respectively. Also we discuss scattering of waves in fluids and solids. Additionally we present the numerical implementation of plane wave transmission experiments in 2-D and 3-D random media using finite-difference solutions of the elastodynamic wave equation (section 2.2). A theoretical and numerical consideration of the probability density functions of wave field fluctuations is given in section (2.3).

2.1 Wave-matter interactions

The variety of methods for description of scattering phenomena is enormous. The here presented outline essentially follows the books of Ishimaru (1978) and Rytov et al. (1987). This work is restricted to the case of wave propagation in continuous random media. The most important partial differential equations and strategies of solution are presented in this section.

2.1.1 Stochastic scalar wave equations

The basic mathematical model for scalar wave propagation in heterogeneous media is the wave equation with random coefficients. In the following, we look for a solution of the acoustic wave equation

$$\triangle u(t,\mathbf{r}) - p^2(\mathbf{r})\frac{\partial^2 u(t,\mathbf{r})}{\partial t^2} = 0 \tag{2.1}$$

with $u(\mathbf{r},t)$ as a scalar wave field and $\triangle$ is the Laplace operator with respect to $\mathbf{r}$. In (2.1) we defined the squared slowness $p^2(\mathbf{r})$ as

$$p^2(\mathbf{r}) = \frac{1}{c_0^2}(1+2n(\mathbf{r})) \quad , \tag{2.2}$$

where c_0 denotes the propagation velocity in a homogeneous reference medium. The function $n(\mathbf{r})$ is a realization of a stationary statistically homogeneous, isotropic random field with zero average, i.e., $\langle n(\mathbf{r})\rangle = 0$. and is characterized by a spatial correlation function

$$B(r) = \langle n(\mathbf{r}_1)n(\mathbf{r}_2)\rangle \tag{2.3}$$

that only depends on the difference coordinate $r = |\mathbf{r}_1 - \mathbf{r}_2|$. The angular brackets denote the ensemble average, i.e the average over all realizations of the random field. Later we make use of the Gaussian correlation function $B(r) = \sigma_n^2 \exp(-r^2/a^2)$ and the exponential correlation function $B(r) = \sigma_n^2 \exp(-|r|/a)$, where σ_n^2 and a denote the variance of the fluctuations and correlation length, respectively. The Fourier transform of the correlation function $B(\mathbf{r}-\mathbf{r}')$ is denoted as the fluctuation spectrum $\Phi(\mathbf{K})$ such that

$$\begin{aligned} B(\mathbf{r}-\mathbf{r}') &= \int d^3\mathbf{K}\,\Phi(\mathbf{K})\,e^{i\mathbf{K}(\mathbf{r}-\mathbf{r}')} \\ \Phi(\mathbf{K}) &= \frac{1}{(2\pi)^3}\int d^3(\mathbf{r}-\mathbf{r}')\,B(\mathbf{r}-\mathbf{r}')\,e^{-i\mathbf{K}(\mathbf{r}-\mathbf{r}')}\,, \end{aligned} \tag{2.4}$$

where $\mathbf{K}$ is the spatial wave vector (for statistical isotropy equations (2.4) simplify accordingly). Here and in the following, integrals without limits imply integration from $-\infty$ to ∞.

In the wave equation (2.1) we can represent the wave field u as Fourier integrals

$$u(t,\mathbf{r}) = \frac{1}{2\pi}\int_{-\infty}^{\infty} d\omega\, U(\omega,\mathbf{r})\,e^{-i\omega t} \tag{2.5}$$

$$U(\omega,\mathbf{r}) = \int_{-\infty}^{\infty} dt\, u(t,\mathbf{r})\,e^{i\omega t}\,. \tag{2.6}$$

Note the different definitions of spatial and temporal Fourier transforms (equations (2.4)-(2.6)) that we use throughout this thesis. Substituting equation (2.5) into wave equation (2.1) and equate the Fourier components we recover the Helmholtz equation

$$\triangle U(\omega,\mathbf{r}) + k^2[1+2n(\mathbf{r})]U(\omega,\mathbf{r}) = 0\,, \tag{2.7}$$

where $k = w/c_0$ is called the wave number.

Using the Green's function approach, the solution of equation (2.7) is

$$U(\omega, \mathbf{r}) = U_0(\omega, \mathbf{r}) + 2k^2 \int d^3\mathbf{r}' G_0(\mathbf{r} - \mathbf{r}') n(\mathbf{r}') U(\omega, \mathbf{r}')\,, \tag{2.8}$$

where U_0 is a solution of equation (2.7) when $n(\mathbf{r}) = 0$ and $G_0(\mathbf{r}-\mathbf{r}')$ is the free space Green's function obeying

$$\triangle G_0(\mathbf{r} - \mathbf{r}') + k^2 G_0(\mathbf{r} - \mathbf{r}') = \delta(\mathbf{r} - \mathbf{r}') \tag{2.9}$$

and satisfying the Sommerfeld radiation conditions, i.e. $G_0(\mathbf{r} - \mathbf{r}') \to 0$ if $|\mathbf{r} - \mathbf{r}'| \to \infty$. In 3-D we have

$$G_0(\mathbf{r} - \mathbf{r}') = \frac{1}{4\pi|\mathbf{r} - \mathbf{r}'|} e^{ik|\mathbf{r}-\mathbf{r}'|}\,. \tag{2.10}$$

Considering now a plane wave propagating in z-direction and breaking down the integration in equation (2.8) with respect to z into $0 < z' < z$ and $z < z' < \infty$, we may interpret solution (2.8) in the sense that the wave field is a superposition of waves scattered on heterogeneities at point $\mathbf{r}'$. Then, the first interval accounts for contributions from forward (positive z-direction) scattered waves since for all locations of scattering points $\mathbf{r}'$ the z-component is smaller than that of the observation point at z. Conversely, the integration interval $z < z' < \infty$ corresponds to wave paths with a least on backscattered event and is neglected in the following. If the wavelength is smaller than the heterogeneities, i.e., $\lambda < a$ then the Green's function can be taken in its Fresnel approximation (Rytov et al., 1989)

$$G_F(\mathbf{r} - \mathbf{r}') = \frac{1}{4\pi(z - z')} e^{ik(z-z') + ik\frac{(\mathbf{r}_\perp - \mathbf{r}'_\perp)^2}{2(z-z')}} \tag{2.11}$$

with the transverse coordinates $\mathbf{r}_\perp$ (directions perpendicular to the direction of propagation z). Substituting this approximation into the remaining part of equation (2.8) we obtain

$$U(\omega, z, \mathbf{r}_\perp) = U_0(\omega, z, \mathbf{r}_\perp) + \frac{k^2}{2\pi} \int_0^z dz' \, \frac{e^{ik(z-z')}}{z - z'} \int d^2\mathbf{r}'_\perp \, e^{ik\frac{(\mathbf{r}_\perp - \mathbf{r}'_\perp)^2}{2(z-z')}} \, n(\mathbf{r}') \, U(\omega, z, \mathbf{r}'_\perp)\,. \tag{2.12}$$

Assuming that the solution of equation (2.12) can be represented by $U(\omega, \mathbf{r}) = v(\omega, \mathbf{r}) \exp(ikz)$ with $U_0 = A_0 \exp(ikz)$ and differentiating equation (2.12) with respect to z yields the parabolic wave equation

$$2ik\frac{\partial v(\omega, \mathbf{r})}{\partial z} + \triangle_\perp v(\omega, \mathbf{r}) + 2k^2 n(\mathbf{r})\, v(\omega, \mathbf{r}) = 0\,, \tag{2.13}$$

where we use

$$\triangle_\perp = \frac{\partial^2}{\partial x^2} + \frac{\partial^2}{\partial y^2}\,. \tag{2.14}$$

Equation (2.13) is also called one-way wave equation. From the above given derivation it becomes clear that equation (2.13) includes multiple forward scattering but neglects backscattering of waves. There are various other strategies to derive the parabolic wave equation (see e.g. Jensen et al., 2000).

2.1.2 Propagation regimes

A commonly used classification scheme of scattering phenomena is presented in Figure (2.1). The $(ka-L/a)$-plane, where ka and L/a denote the normalized frequency and travel-distance (k is the wave number, L the travel-distance and a the characteristic size of the heterogeneities), is divided in various sub-regimes briefly discussed in the following.
For $ka \ll 1$ the scattered power is proportional to k^{d+1}, where d denotes the spatial dimension. This regime is known as *Rayleigh scattering.*
For $ka \approx 1$ the sizes of heterogeneities are comparable to the wavelength. Since the incident waves are scattered with large angles relative to the incident direction, this regime is called *large angle scattering.* It is also known as *resonance* or *Mie scattering* regime.
For $ka > 1$ the power of the waves is scattered predominantly in the forward direction. Hence, it is called *small angle scattering.* The small angle scattering problem may be further divided into three sub-regimes that are characterized by the wave parameter D and the scattering strength S:

$$D = \frac{2L}{ka^2} \tag{2.15}$$

$$S = \sigma_n \zeta ka \sqrt{L/a}\,, \tag{2.16}$$

where $\zeta = a_z/a$ with a_z the characteristic scale in propagation direction. σ_n is called the perturbation strength. In this thesis σ_n can be approximately understood as the standard deviation of the velocity fluctuations. Note that the wave parameter is defined as $D \propto \kappa_m^2/\kappa_F^2$ where κ_m is the spatial wave number corresponding to the size of the smallest inhomogeneity (in our case of a single scale medium $\kappa_m = \frac{2\pi}{a}$) and κ_F is the spatial wave number corresponding to the first Fresnel zone (which is for plane waves $\sqrt{\lambda L}$). Therefore, D serves as an indicator whether diffraction effects have to be taken into account or not. The scattering strength S essentially serves as a measure of the strength of fluctuations. Note that S^2 is related to the mean square phase fluctuations and is also called optical distance (Ishimaru, 1978). In terms of these parameters the following regimes may be defined

- *Geometrical optics*: this regime is limited by $ka > 1$, $D < 1$ and $SD < 2\pi$. Then the eikonal and the transport equations can be used for the description of wave propagation in inhomogeneous media.

- *Diffraction regime*: this regime is limited by $ka > 1$, $D > 1$ and $S < 2\pi$. Diffraction refers to the propagation of waves almost but not quite along straight lines.

- *Saturated regime*: is defined by the two lines $S > 2\pi$ and $SD > 2\pi$. Multiple scattering becomes more and more important. Adequate concepts include the radiative transport theory and the diffusion approximation. Interference of multiply scattered waves lead to the effect of coherent backscattering (see Figure (2.2) for illustration) and eventually to the localization of waves, i.e. the wave field energy becomes trapped within exponentially small spatial domains (Sheng, 1995).

For line-of-sight scattering problems that are treated in this thesis a somewhat different distinction between weak and strong wave field fluctuation regimes is usual (Ishimaru, 1978). Here the wave field can be thought as a sum of coherent and a fluctuating wave field

$$u = \langle u \rangle + u_f \tag{2.17}$$

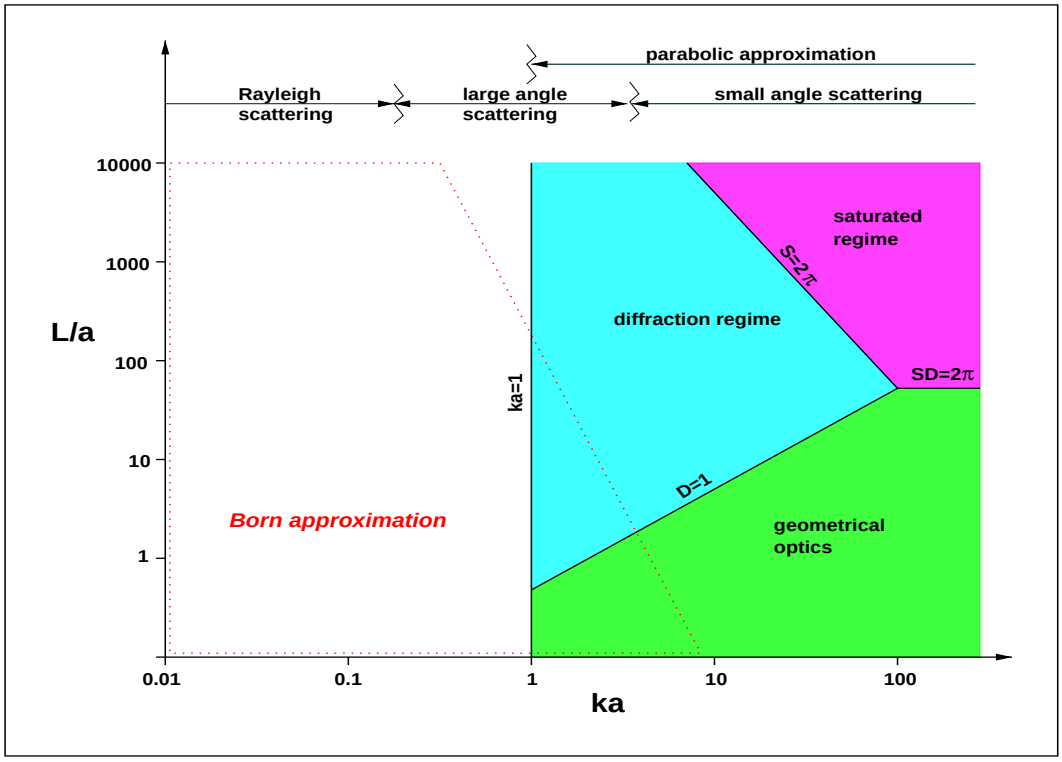

Figure 2.1: Scattering regimes classified in the $(ka - L/a)$-plane (simplified re-plot of Figure (1) in Wu and Aki (1988)). Note that the lines $S = 2\pi$ and $SD = 2\pi$ actually depend on the perturbation strength σ_n. In this plot we used $\sigma_n = 10\%$.

and also the total intensity can be expressed as

$$\begin{aligned} I_t &= \langle |u|^2 \rangle && (2.18)\\ &= |\langle u \rangle|^2 + \langle |u_f|^2 \rangle && (2.19)\\ &= I_c + I_f \,. && (2.20) \end{aligned}$$

A simple measure of the strength of the wave field fluctuations is then given by the ratio

$$\epsilon = \frac{|u_f|}{|\langle u \rangle|} \,. \tag{2.21}$$

Small values of ϵ indicate that the coherent wave dominates. In the weak wave field fluctuation regime ϵ is a small parameter so that its variance $\langle \epsilon^2 \rangle$ is much smaller than unity. Conversely, the case, where the fluctuating wave field is of the order of the coherent wave field, is called the strong wave field fluctuation regime. Later, we shall use this small parameter ϵ to express the order of accuracy of wave field attributes. Another measure is the scintillation index

$$m^2 = \frac{\langle (I - \langle I \rangle)^2 \rangle}{\langle I \rangle^2} \,, \tag{2.22}$$

where I is the intensity of the recorded wave field. The intensity fluctuations saturate when both S and SD are greater than order unity.

The following subsection introduces methods for the weak and strong wave field fluctuation case based on the partial differential equations presented in (2.1.1).

2.1.3 Methods for weak and strong wave field fluctuations

In the weak wave field fluctuation regime several methods exist to derive approximate solutions to equations (2.1), (2.7) and (2.13). We briefly discuss the most important methods that are used in this thesis. We also mention approximations in the case of strong wave field fluctuations.

Born approximation

The well-known Born approximation we already encountered. The Green's function approach – applied to solve the Helmholtz equation (2.7) – yields immediately the scattering series. The first order Born approximation is obtained by replacing $U(\omega, \mathbf{r}')$ in the integral of equation (2.8) by U_0 i.e. the field in the absence of the fluctuations:

$$U_{Born}(\omega, \mathbf{r}) = U_0(\omega, \mathbf{r}) + 2k^2 \int d^3\mathbf{r}' G(\mathbf{r} - \mathbf{r}') n(\mathbf{r}') U_0(\omega, \mathbf{r}') \,. \tag{2.23}$$

Its range of applicability can be expressed as

$$\sigma_n^2 ka \frac{L}{a} \ll 1 \tag{2.24}$$

and is illustrated in Fig. (2.1) by the red dots. Inequality (2.24) can be satisfied in two cases: First, if the wavelength is much larger than the scattering volume (the volume, where $n(\mathbf{r}) \neq 0$) so that $kL \ll 1$ then it does not matter whether the heterogeneities are strong or not. Second, the heterogeneities are so weak ($\sigma_n^2 \ll 1$) that the wave can even propagate over long travel-distances.

Bourret approximation

Substituting the free space Green's function G_0 into (2.8) and write the iteration in an explicit form with $U_0(\mathbf{r}) = G_0(\mathbf{r}, \mathbf{r}_0)$ we obtain the full scattering series

$$\begin{aligned} G(\mathbf{r}, \mathbf{r}_0) \;=\; & G_0(\mathbf{r}, \mathbf{r}_0) + 2k^2 \int d^3\mathbf{r}_1 \, G_0(\mathbf{r}, \mathbf{r}_1) n(\mathbf{r}_1) G_0(\mathbf{r}_1, \mathbf{r}_0) \\ & + 4k^4 \iint d^3\mathbf{r}_1 d^3\mathbf{r}_2 \, G_0(\mathbf{r}, \mathbf{r}_1) n(\mathbf{r}_1) G_0(\mathbf{r}_1, \mathbf{r}_2) n(\mathbf{r}_2) G_0(\mathbf{r}_2, \mathbf{r}_0) \\ & + 8k^6 \iiint d^3\mathbf{r}_1 d^3\mathbf{r}_2 d^3\mathbf{r}_3 \, G_0(\mathbf{r}, \mathbf{r}_1) n(\mathbf{r}_1) G_0(\mathbf{r}_1, \mathbf{r}_2) n(\mathbf{r}_2) G_0(\mathbf{r}_2, \mathbf{r}_3) G_0(\mathbf{r}_3, \mathbf{r}_0) \\ & + \;\; \ldots \;\; . \end{aligned} \tag{2.25}$$

Equation (2.25) has a clear physical interpretation because it corresponds to a decomposition of the wave field into the number of scattering events involved. So, the first term is the free space Green's function and represents the unscattered wave. The second term is the single scattering contribution, the third term corresponds to two-fold scattering etc..

If $n(\mathbf{r})$ is a Gaussian random field, then the odd statistical moments of $n(\mathbf{r})$ vanish and the even moments can be expressed as combinations of the second moment

$$\langle n(\mathbf{r}_1) .. n(\mathbf{r}_{2n}) \rangle = \sum_{pp} B(\mathbf{r}_\alpha, \mathbf{r}_\beta) \cdot .. \cdot B(\mathbf{r}_\gamma, \mathbf{r}_\delta) \,, \tag{2.26}$$

where the sum extends over all possible pairs $(\mathbf{r}_\alpha, \mathbf{r}_\beta)$. Using this relation we obtain for the ensemble averaged Green's function

$$\begin{aligned}\langle G(\mathbf{r},\mathbf{r}_0)\rangle &= G_0(\mathbf{r},\mathbf{r}_0) + 4k^4 \iint d^3\mathbf{r}_1 d^3\mathbf{r}_2\, G_0(\mathbf{r},\mathbf{r}_1) G_0(\mathbf{r}_1,\mathbf{r}_2) G_0(\mathbf{r}_2,\mathbf{r}_0) B(\mathbf{r}_1,\mathbf{r}_2) \\ &\quad + 16k^8 \iiint\!\!\iint d^3\mathbf{r}_1 d^3\mathbf{r}_2 d^3\mathbf{r}_3 d^3\mathbf{r}_4\, G_0(\mathbf{r},\mathbf{r}_1) G_0(\mathbf{r}_1,\mathbf{r}_2) G_0(\mathbf{r}_2,\mathbf{r}_3) G_0(\mathbf{r}_3,\mathbf{r}_4) G_0(\mathbf{r}_4,\mathbf{r}_0) \\ &\qquad\qquad [B(\mathbf{r}_1,\mathbf{r}_2)B(\mathbf{r}_3,\mathbf{r}_4) + B(\mathbf{r}_1,\mathbf{r}_3)B(\mathbf{r}_2,\mathbf{r}_4) + B(\mathbf{r}_1,\mathbf{r}_4)B(\mathbf{r}_2,\mathbf{r}_3)] \\ &\quad + \quad \ldots \quad . \end{aligned} \tag{2.27}$$

Each term in this series refers to a certain order of scattering. Rearranging the terms in (2.27), it can be written as an iteration, which is called the Dyson equation

$$\langle G(\mathbf{r},\mathbf{r}_0)\rangle = G_0(\mathbf{r},\mathbf{r}_0) + \iint d^3\mathbf{r}_1 d^3\mathbf{r}_2\, G_0(\mathbf{r},\mathbf{r}_1) Q(\mathbf{r}_1,\mathbf{r}_2) \langle G(\mathbf{r}_2,\mathbf{r}_0)\rangle \tag{2.28}$$

with

$$\begin{aligned} Q(\mathbf{r}_1,\mathbf{r}_2) &= 4k^2 G_0(\mathbf{r}_1,\mathbf{r}_2) B(\mathbf{r}_1,\mathbf{r}_2) \\ &\quad + 16k^8 \iint d^3\mathbf{r}' d^3\mathbf{r}''\, G_0(\mathbf{r}',\mathbf{r}_1) G_0(\mathbf{r}',\mathbf{r}'') G_0(\mathbf{r}'',\mathbf{r}_2) B(\mathbf{r}_1,\mathbf{r}'') B(\mathbf{r}',\mathbf{r}_2) \\ &\quad + \quad \ldots \quad . \end{aligned} \tag{2.29}$$

Explicit solutions of the Dyson equation are not available, but several approximations exist (Rytov et. al, 1989). So, the Bourret approximation keeps only the first term of Q. For statistically homogeneous media this leads to

$$Q(\mathbf{r}_1 - \mathbf{r}_2) \approx 4k^4 G_0(\mathbf{r}_1 - \mathbf{r}_2) B(\mathbf{r}_1 - \mathbf{r}_2)\,. \tag{2.30}$$

Now, explicit solutions of equation (2.28) can be obtained. In the case of 3-D statistically isotropic media the solution is of the form

$$\langle G(r)\rangle = \frac{e^{i\tilde{k}r}}{4\pi r} \tag{2.31}$$

with an effective, complex wave number

$$\tilde{k} = k\left[1 + k\int_0^\infty dr\, B(r)\sin(2kr) + 2ik\int_0^\infty dr\, B(r)\sin^2(kr)\right] \tag{2.32}$$

and $r = |\mathbf{r}_1 - \mathbf{r}_2|$. For detailed calculations we refer to Rytov et al., 1989. For the 2-D case also explicit results have been obtained (Shapiro et al., 1996b). The solution (2.31) describes the mean Green's function corresponding to a coherent wave field. The imaginary part of the effective wave number results in an exponential decay of the coherent wave field, whereas its real part is related to the coherent phase. A graphical interpretation of the Bourret approximation can be seen in Fig. (2.2). Its range of applicability is classically denoted by $\sigma_n^2 (ka)^2 \ll 1$. Recent results indicate that the Bourret approximation has a wider range of applicability (Samelsohn and Mazar, 1996). They provide the restriction

$$ka^2 \ll L \qquad \rightleftharpoons \qquad D \gg 1\,. \tag{2.33}$$

Rytov approximation

The Rytov method is based on the the parabolic wave equation (2.13), where the wave field $U(\omega, \mathbf{r})$ and the complex function $v(\omega, \mathbf{r})$ are related by

$$U(\omega, \mathbf{r}) = v(\omega, \mathbf{r}) e^{ikz} \,. \tag{2.34}$$

$U(\omega, \mathbf{r})$ represents the wave field inside the random medium when the incident plane wave is of the form

$$U_0(\omega, z) = A_0 e^{i\phi_0} \,, \tag{2.35}$$

i.e., a plane wave with constant amplitude propagating in z-direction such that $\phi_0 = kz$. If we choose v such that it expresses the fluctuations of amplitudes and phase relative to the incident wave U_0, one can represent v as

$$\begin{aligned} v(\omega, \mathbf{r}) &= A_0 e^{\ln(A(\omega,\mathbf{r})/A_0) + i(\phi(\omega,\mathbf{r}) - \phi_0)} & (2.36) \\ &= A_0 e^{\Psi(\omega,\mathbf{r})} \,, & (2.37) \end{aligned}$$

where the complex exponent is usually expressed by $\Psi = \chi + i\tilde{\phi}$ with $\chi = \ln(A/A_0)$ and $\tilde{\phi} = \phi - \phi_0$ which are the so-called log-amplitude and phase fluctuations, respectively.

Substituting equation (2.36) into the parabolic wave equation we obtain a nonlinear, partial differential equation for the complex exponent Ψ

$$2ik \frac{\partial \Psi(\omega, \mathbf{r})}{\partial z} + \triangle_\perp \Psi(\omega, \mathbf{r}) + [\nabla_\perp \Psi(\omega, \mathbf{r})]^2 + k^2 n(\mathbf{r}) = 0 \tag{2.38}$$

with the nabla operator corresponding to the transverse coordinates

$$\nabla_\perp = \begin{pmatrix} \partial/\partial x \\ \partial/\partial y \end{pmatrix} . \tag{2.39}$$

The solution of equation (2.38) together with equation (2.34) describes the wave field inside the random medium. In appendix A we derive a solution of equation (2.38) by an expansion of Ψ. For an alternative derivation of the Rytov approximation based on the Green's function approach we refer to Ishimaru (1978).

The applicability of Rytov's method is generally limited by the weak wave field fluctuation regime ($\langle \epsilon^2 \rangle \ll 1$). If the fluctuations of the medium are weak, the Rytov and Born approximation practically coincide (see e.g. Keller, 1969). Therefore, the Rytov approximation is applicable in all displayed regimes of Fig. (2.1) apart from the saturated regime. This is also pointed out by Dashen (1979). To interpret the solution of Rytov's method we must take into account that it is based on the parabolic wave equation, neglecting all backscattered waves. This is also illustrated in Fig. (2.2).

Markov approximation

Starting from the parabolic wave equation, the Markov approximation leads to partial differential equations for the statistical moments (of arbitrary order) of wave fields. An essential assumption of the Markov approximation is that the random field is δ-correlated in the direction of propagation:

$$\langle n(z', \mathbf{r}_\perp) n(z', \mathbf{r}'_\perp) \rangle = \delta(z - z') A(\mathbf{r}_\perp - \mathbf{r}'_\perp) \,, \tag{2.40}$$

where A is the 2-D Fourier transform of the fluctuation spectrum

$$A(\mathbf{r}_\perp - \mathbf{r}'_\perp) = 2\pi \int d\kappa\, \Phi(\kappa) e^{i\kappa(\mathbf{r}_\perp - \mathbf{r}'_\perp)}\,. \tag{2.41}$$

Note that this assumption implicitly requires the existence of an directionally ordered space variable like the main propagation direction of a plane wave (Rytov et al., 1989). Explicit results for the mean field and the second moment

$$\Gamma_2(\omega', \omega'', z, \mathbf{r}'_\perp, \mathbf{r}''_\perp) = \langle U(\omega', z, \mathbf{r}'_\perp) U^\star(\omega'', z, \mathbf{r}''_\perp)\rangle \tag{2.42}$$

are available as shown in detail in Sato and Fehler, 1998, Ishimaru, 1978, and Rytov et al., 1989 ($U^\star$ denotes the complex conjugation of U). Γ_2 is the so-called two-frequency mutual coherence function which we shall use in chapter (4). It describes the wave field correlation between two locations $\mathbf{r}'_\perp$, $\mathbf{r}''_\perp$ and two frequencies ω', ω''. A solution for Γ_2 for 2-D random media is derived in appendix D.

The derivation of the Markov equations is not based on the assumption of small wave field fluctuations. However, the parabolic wave equation permits no backscattering and therefore the Markov approximation either. That means the Markov approximation is a suitable wave field description (even in the saturated regime) as long as backscattered wave can be neglected. A quantitative discussion of its range of applicability is given in Rytov et al. (1989) which leads to

$$\sigma_n^2 k^2 a_z^2 \ll 1\,, \tag{2.43}$$

where a_z denotes the correlation length in the direction of propagation.

Another approach to solve the parabolic wave equation is the method of path-integrals using infinite dimensional integrals (Dashen, 1979). Explicit solutions for the first and second statistical moment of the wave field coincide with the solutions derived in the Markov approximation.

Other approaches

In the saturated regime there is a phenomenological theory of radiative transport which describes the propagation of the intensity through the random medium. The transport equation is used in seismology in order to model coda waves (Sato and Fehler, 1998). In this regime the correlation length becomes less relevant and the mean free path is introduced as a new scale in the description of scattering phenomena. For large travel-distances (relative to the mean free path) the transport equation can be approximated by a diffusion equation. However, in spite of such an approximation the diffusive transport of waves must be somewhat different from classical diffusion like heat conduction. This is because the causality principle is not valid in this context (but it should be since multiply scattered waves also obey the causality principle (Weaver, 1986)). Another deviation from classical diffusion is the effect of coherent backscattering (Sheng, 1995) which is generally understood as a precursor to wave localization.

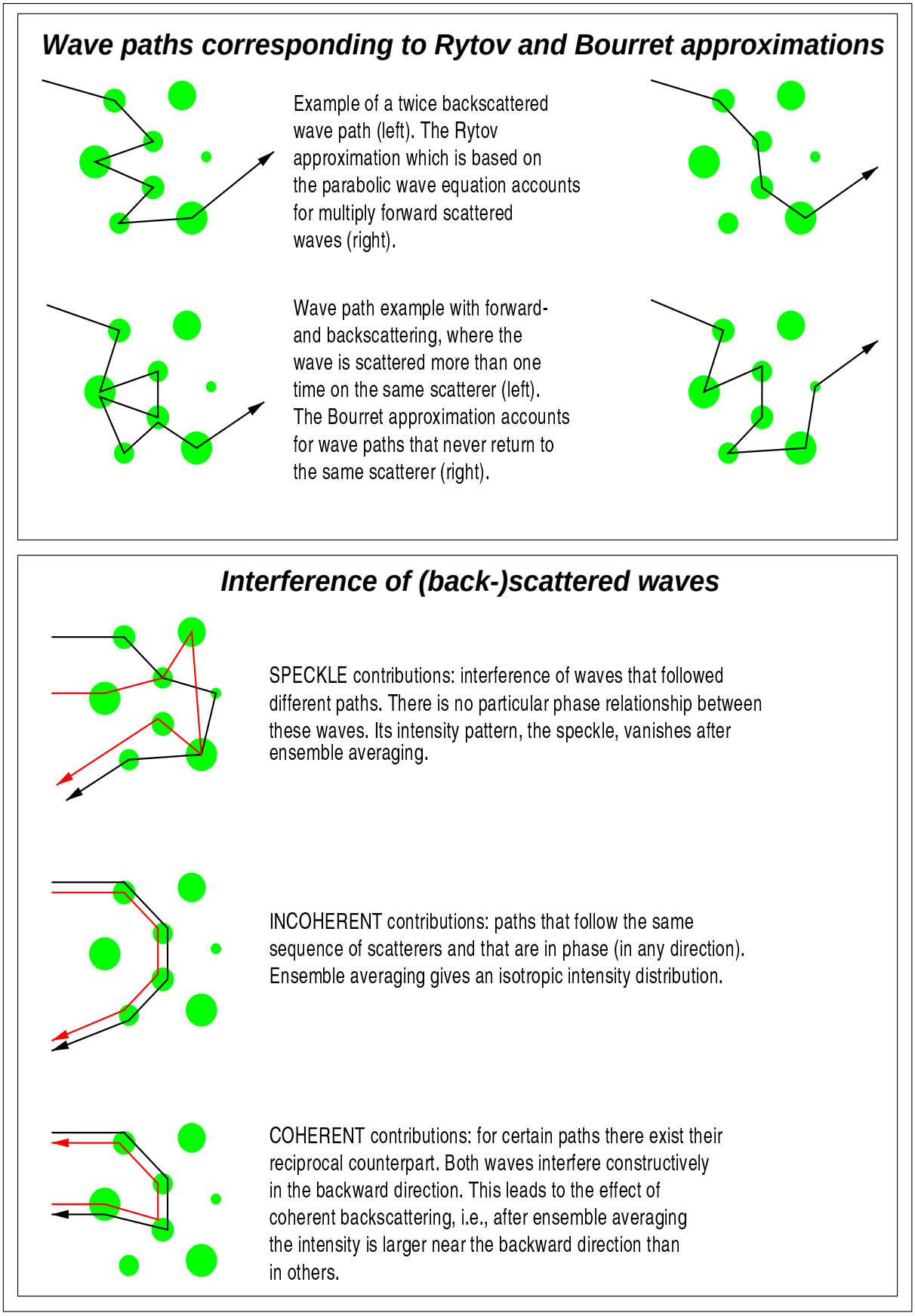

Figure 2.2: Explanation of wave phenomena with path theory.

2.1.4 Vector versus scalar wave scattering

A rigorous description of wave propagation and scattering in the solid Earth must be based on the elastodynamic wave equation (see e.g. Aki and Richards, 1980)

$$\rho(\mathbf{r})\ddot{u}_i(t,\mathbf{r}) = [c_{ijkl}(\mathbf{r})u_{k,l}(t,\mathbf{r})]_{,j} \quad , \tag{2.44}$$

where the stiffness tensor in isotropic media (we are dealing with exclusively in this study) is given by

$$c_{ijkl}(\mathbf{r}) = \lambda(\mathbf{r})\delta_{ij}\delta_{kl} + \mu(\mathbf{r})\delta_{ik}\delta_{jl} + \mu(\mathbf{r})\delta_{il}\delta_{jk} \tag{2.45}$$

and λ, μ are the Lamé parameters, ρ is the density; δ_{ij} is the Kronecker symbol. Summation over repeated indices is assumed and $_{,i}$ means the partial derivative with respect to the ith coordinate. In contrast to the scalar wave equation, the elastodynamic wave equation describes multi-mode wave propagation. Therefore, when dealing with scattering problems one has to take into account the conversion from one wave mode into another (e.g. P $\rightarrow$ S).

The above presented perturbation techniques can be used provided that their are properly extended. We follow the review article of Wu (1988) in order discuss the similarity and differences of perturbation methods for wave propagation in weakly heterogeneous fluids and solids. Note that the following numerical experiments simulate wave propagation in solids. Accordingly we have to apply the elastic extensions of the used perturbation methods. For a review we refer to Gold (1997) who derived the elastic Bourret and Rytov approximation. The results are also summarized in appendix E. A recent discussion of the elastic Born approximation can be found in Kirchner (2000).

A useful quantity in order to describe the scattering characteristics of a wave entering a region of discrete point scatterers is the scattering coefficient g. It is defined by $g = 4\pi n\frac{d\sigma}{d\Omega}$, $\frac{d\sigma}{d\Omega}$ is the differential scattering cross section and n is the number density of scatterers. Since we are dealing with randomly inhomogeneous, continuous media it is necessary to compute the ensemble averaged differential scattering cross section $\langle\frac{d\sigma}{d\Omega}\rangle$ and to achieve the transition from discrete to continuous random media. This calculation is presented in detail in Chernov (1960) and Sato & Fehler (1998), where the scattered wave field is represented in the Born approximation. For scalar wave propagation in isotropic random media the scattering coefficient is given by

$$g(\vartheta,k) = \frac{k^4}{\pi}\,\Phi(2k\sin(\vartheta/2))\,. \tag{2.46}$$

The scattering coefficient describes the angular dependence of the scattered power as a function of the scattering angle ϑ (the angle between the direction of the incident wave and that of the scattered wave as shown in Figure 2.3) and wave number k. Moreover, g is dependent on the fluctuation spectrum of the media heterogeneities Φ.

The upper half of Figure (2.4) shows in a polar-plot the angular dependence of g for a 3-D exponentially correlated random medium for different normalized frequencies. For isotropic media, g is axially symmetric with respect to the incident wave direction. Only for low frequencies ($ka \ll 1$) g is symmetric with respect to the origin. That is to say the same amount of wave power is scattered in all directions. For frequencies $ka > 1$ the

power is scattered mainly in the forward direction. Note that this is equivalent to the small (scattering) angle regime.

The same strategy can be used in order to calculate the scattering coefficient for elastic random media. Instead of a single function g in the scalar case, one has now 4 functions: g^{PP} characterizing the scattering of a P-wave into a P-wave, g^{PS} characterizing the scattering of a P-wave into a S-wave ('conversion scattering') and analogously g^{SS}, g^{SP}. All elastic scattering coefficients have a similar structure

$$g^{YY}(\vartheta, \zeta, k) \propto k^4 \, |X(\vartheta, \zeta)|^2 \, \Phi(\vartheta, \zeta, k) \,, \tag{2.47}$$

where X is called the 'scattering pattern' and depends in general on the direction of the scattered wave. ζ is the angle between the x-axis and and the projection of the scattered wave vector into the x, y plane. Explicit expressions are given in Wu (1988) and Sato & Fehler (1998). Principle features of the elastic scattering coefficients are displayed in Figures (2.4) – (2.6).

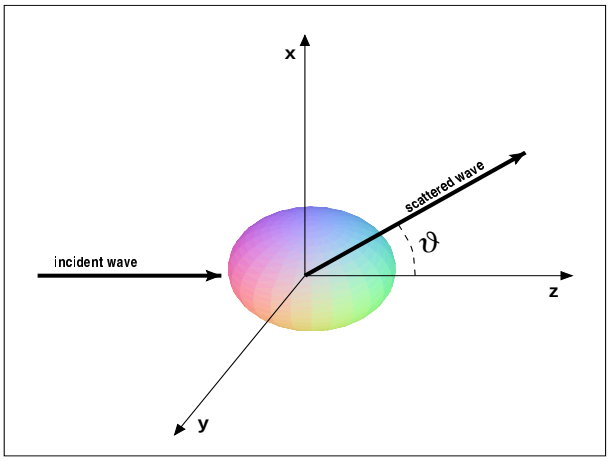

Figure 2.3: Scattering geometry. ϑ is the angle between the incident wave vector and that of the scattered wave.

Forward scattering assumption

The Rytov as well as the Markov approximation are based on the assumption of forward or small-angle scattering (see also the assumptions made in order to derive the parabolic wave equation). The above discussion shows that for $ka \geq 1$ that is the wavelength is smaller than the characteristic size of heterogeneity, the forward scattering assumption is not a crucial one. This applies for both, scalar and vector waves. In this regime, the conversion scattering can be also neglected without significant lack of precision. For $ka < 1$ the amount of backscattered energy becomes more important. Moreover, in the elastic case the conversion from P- to S-waves and vice versa should be taken into consideration.

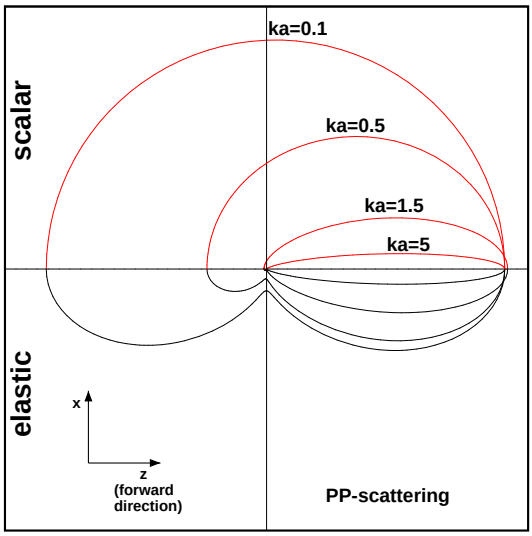

Figure 2.4: The upper half shows the angular dependence of the scalar scattering coefficient for an exponentially correlated random medium. For increasing frequencies ka, the scattered power is confined within a small cone around the forward direction. The lower half of the plot shows g^{PP} for the same ka values. Here we used $v_P/v_S = \sqrt{3}$ and assumed the density to be constant. Furthermore, the P- and S-wave velocity fluctuations are characterized by a single random field. A constant factor $\propto \sigma_n^2/a$ is omitted. Since we are only interested in the angular dependence of g, each curve is multiplied by $1/(ka)^4$. This scaling allows the illustration in a single polar-plot.

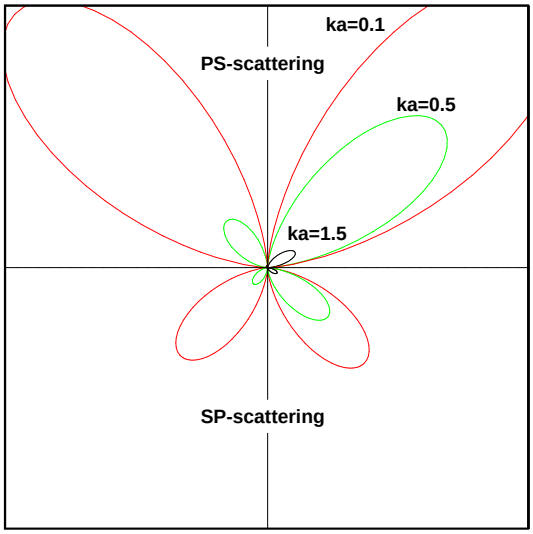

Figure 2.5: The scattering coefficients g^{PS} and g^{SP} are shown in the upper and lower half of the plot, respectively. The parameterization is the same as in Figure (2.4). Note that g^{PS} is expressed as a function of the P-wave number Generally, the same angular dependence of g^{PS} and g^{SP} can be observed. The different size of the lobes can be explained by the following. It can be shown by integration over the solid angle Ω that $\int_{4\pi} g^{PS} d\Omega \approx 2\left(\frac{v_P}{v_S}\right)^2 \int_{4\pi} g^{SP} d\Omega$. As a consequence, P-waves scatter more readily to S-waves than S-waves to P-waves.

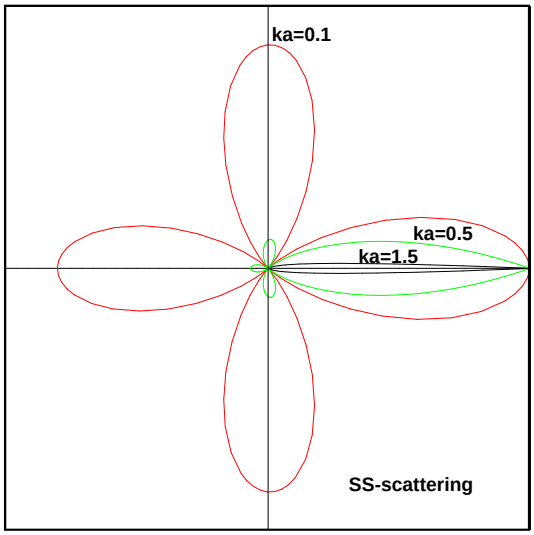

Figure 2.6: The scattering coefficient g^{SS} is shown for $ka = 0.1, 0.5, 1.5$. The parameterization is the same as in Figure (2.4). Note that we expressed g^{SS} as a function of the P-wave number k. In general, g^{SS} is also dependent on the angle ζ which we set to zero in this plot.

2.2 Numerical modeling of waves in elastic random media

2.2.1 Random media realizations in 2-D and 3-D

Random media are a special class of heterogeneous media. They are determined by random variables or random fields like the (stochastic) process in equation (2.2). Hence, the properties of the random medium are defined by the statistical properties of the stochastic process. Here we consider random media that are characterized by the the second-order statistics. That means the realizations of the random medium have a certain mean value and a spatial correlation function defined by the correlation length and the variance.

A random medium realization is generated by taking the inverse Fourier transform of the spectrum of normally distributed fluctuations (with a Gaussian probability density function with zero mean and unit variance) multiplied with the square root of the fluctuation spectrum. Note however, that theory we are going to derive is not based on the assumption of normally distributed fluctuations. Realizations of Gaussian and exponentially correlated random media and their properties are displayed in Fig. (2.7).

2.2.2 Simulation of wave propagation using finite-difference methods

We simulate a plane wave propagating from the top down to a certain depth (z-direction) in a single random medium realization. Similar transmission simulations in acoustic random media were performed by Frankel and Clayton (1986), Kneib and Kerner (1993), Korn (1993), Shapiro et al. (1996b) and by Frenje and Juhlin (2000). For the numerical computation of the wave field we use the so-called rotated-staggered grid finite-difference scheme for the elastodynamic wave equation (Saenger et al., 2000). The computations are performed with 8th-order spatial FD operators and with a second-order time update. Finite-difference simulations in 3-D elastic random media have been performed by Bohlen and Milkereit (2001) using a velocity-stress method and are also used for the following analysis.

The geometry as well as the medium parameters are of the order of reservoir scales and reservoir rocks in the hydrocarbon exploration, respectively. The geometry of the experiment is schematically shown in Figure (2.8). The background medium is characterized by a P-wave velocity of $v_P = 3000m/s$, a S-wave velocity of $v_S = 1850m/s$ and a density of $\rho = 2.5g/\mathrm{cm}^3$. In the actual FD-model the random medium is embedded in a constant background medium with the properties defined above. We choose the model geometry in such a way that undesired reflections from the model borders are excluded. For the modeling we need instead of velocities the stiffness tensor components $c_{1111} = v_P^2\rho$ and $c_{3131} = v_S^2\rho$ and density. For simplicity, only the stiffness tensor component c_{1111} exhibits exponentially correlated fluctuations. We simulate a line-source exhibiting only a z-component. Note that under these conditions no S-waves will be generated. The wavelet is the second derivative of a Ricker-wavelet with a dominant frequency of about 75 Hz and maximum frequency of $\approx 200Hz$ (this corresponds to a dominant wavelength of 40 m for the P-wave). Furthermore, we fulfill the stability criterion required for the rotated staggered grid in each point of the random medium using a time increment of $\Delta t = 9.8 \cdot 10^{-5}s$ and space increment of $\Delta x = 2m$. This results in a discretization of approximately 20 grid points per wavelength and a minimized numerical dispersion.

The wave field is recorded by several receiver lines (where each line consists of 146 receivers) which are placed at several depths positions such that the mean propagation direction of

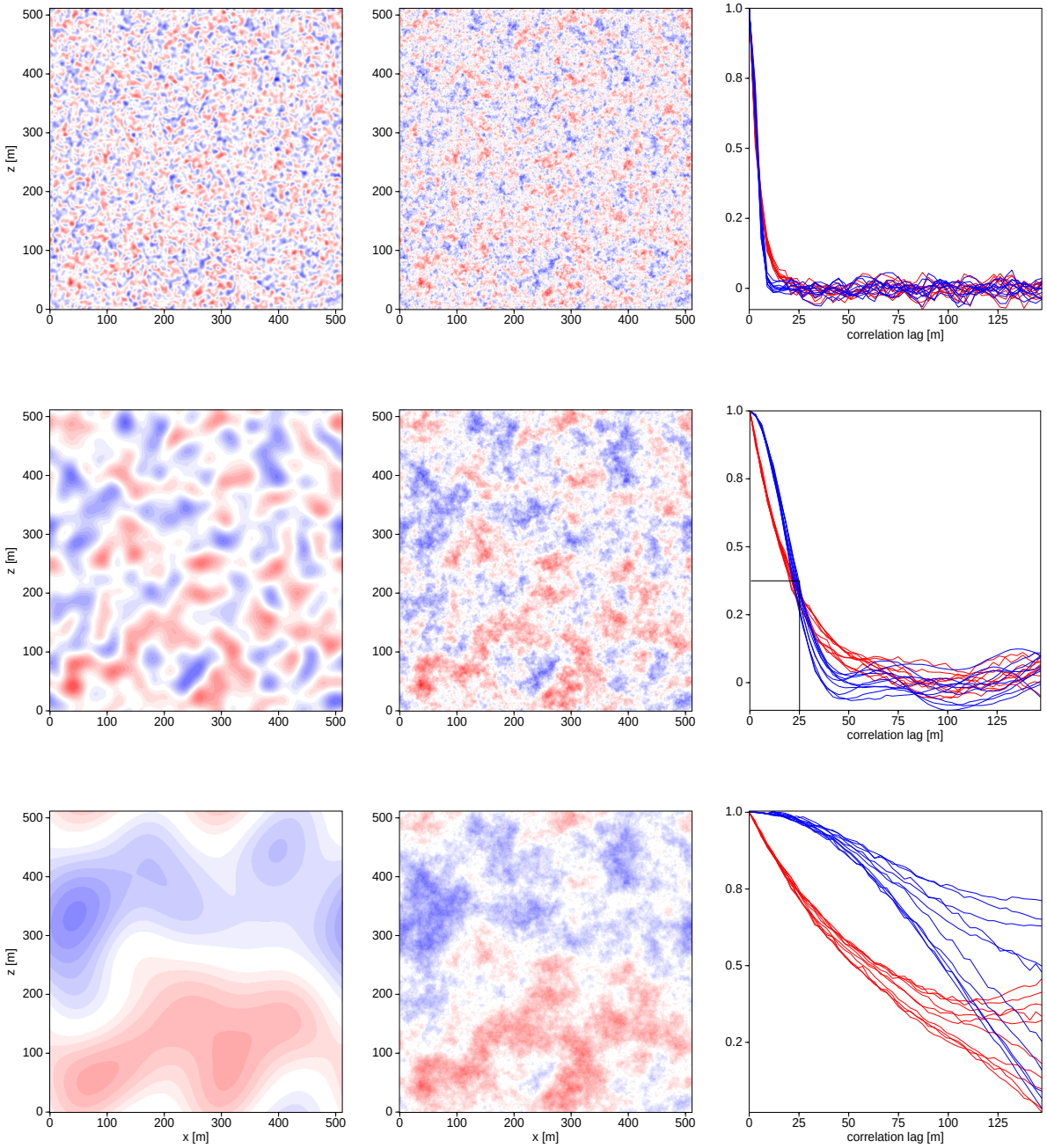

Figure 2.7: Gaussian and exponentially correlated random media realizations are displayed in the first and second column, respectively. From top to bottom the correlation length increases (top: $a = 5m$, middle: $a = 25m$, bottom: $a = 125m$). In the right column are shown the corresponding numerically obtained correlation functions computed for 10 different directions. That the desired spatial correlation property indeed corresponds to the created random media is shown for the case $a = 25m$: for correlation lag $25m$ the correlation function assumes the value $1/e$ as it should be for exponentially and Gaussian correlated random media.

the plane wave and the receiver lines are perpendicular. The lower part of Figure (2.8) additionally displays snapshots of the wave field. The initially undistorted plane wave results in wave fields of increasing complexity due to scattering on the random heterogeneities (from left to right). Recorded seismograms are shown in Figure (2.9).

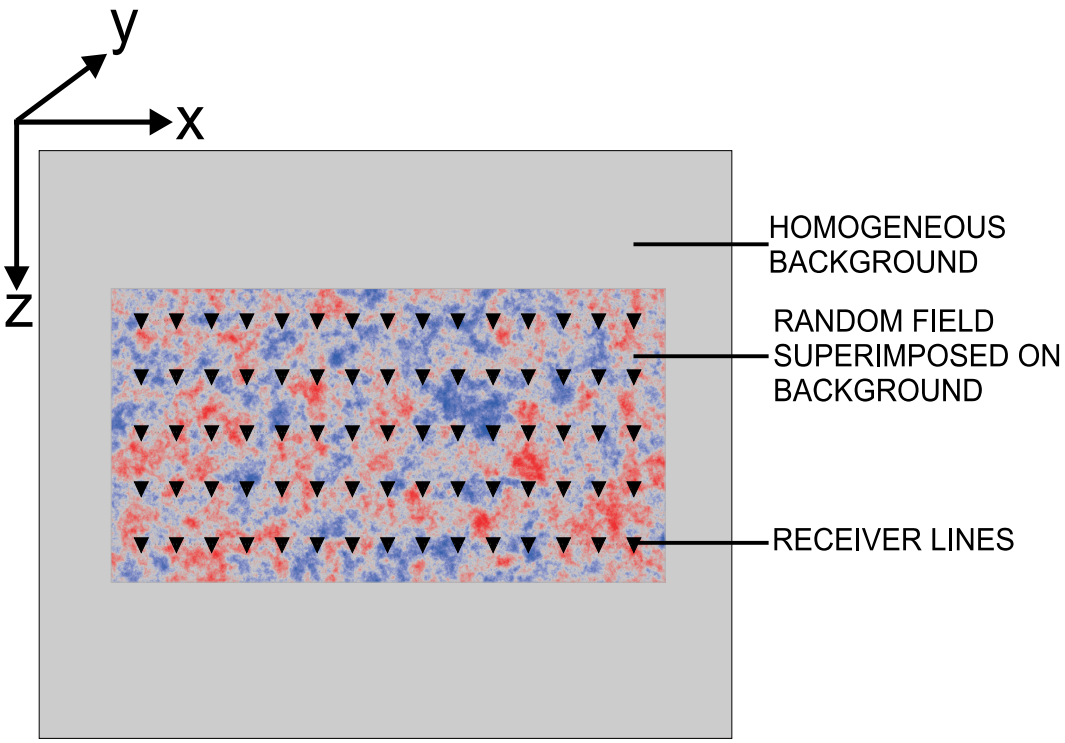

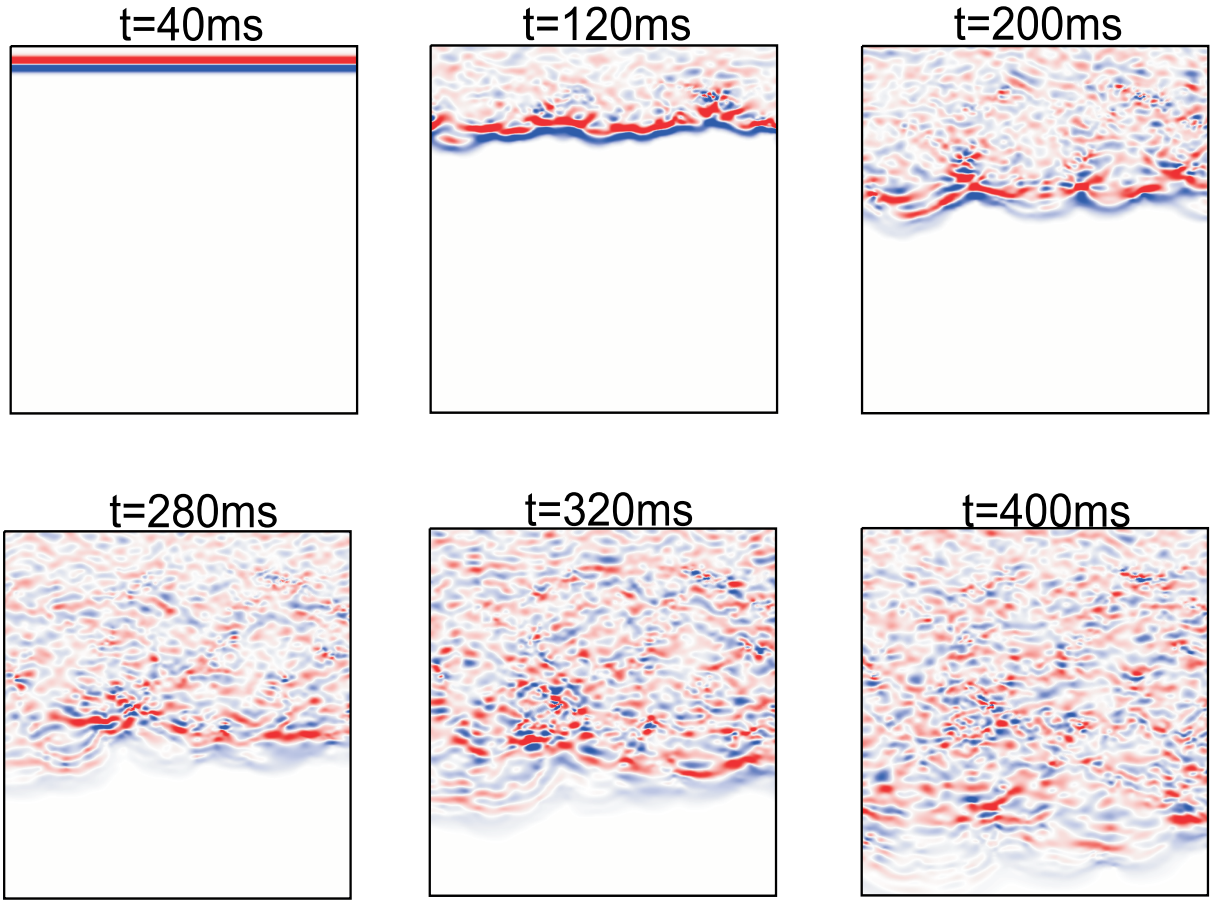

Figure 2.8: Schematic outline of the geometry of the numerical experiment. Below are shown 6 snapshots of the wave field propagating in z-direction in the random medium.

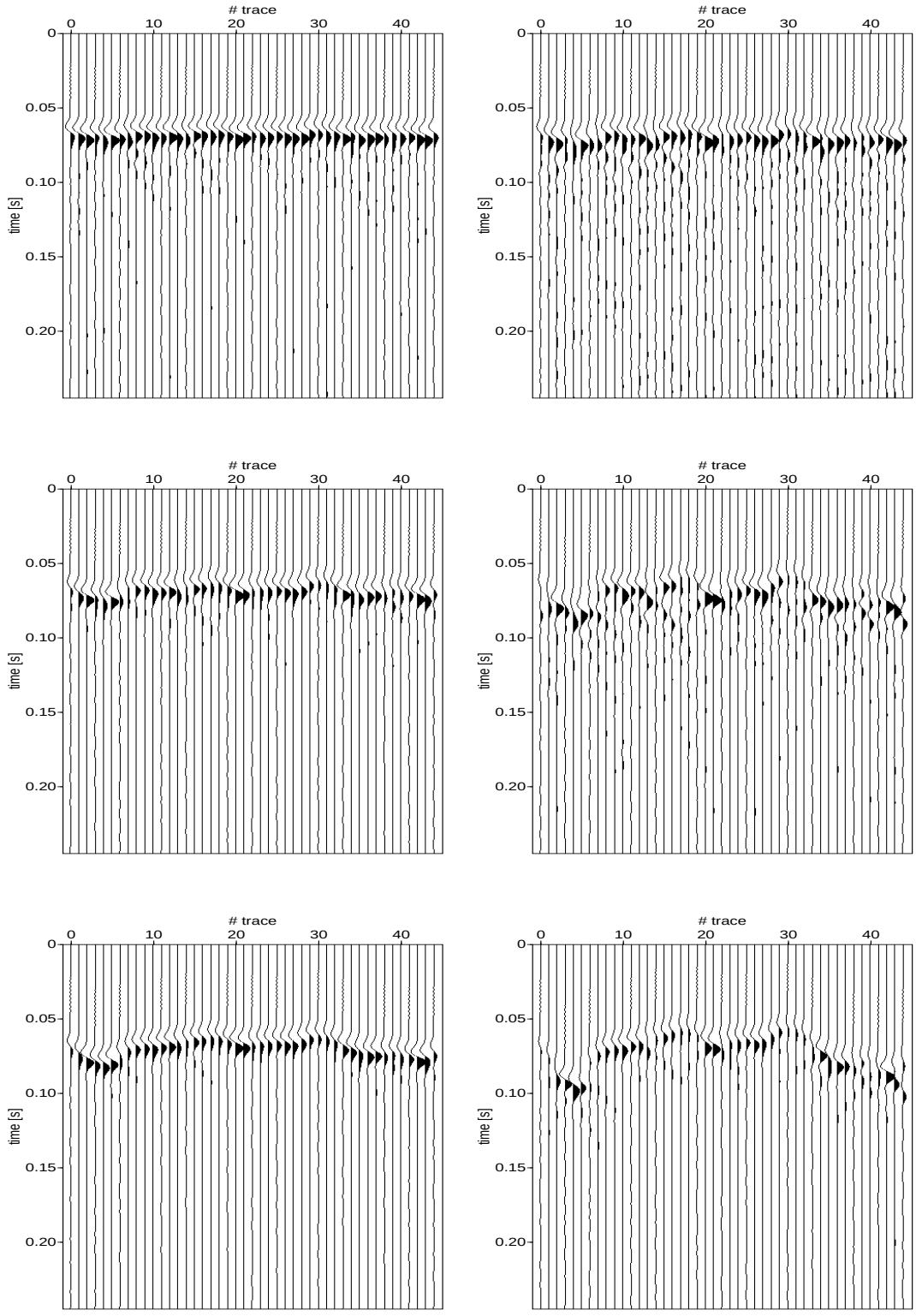

Figure 2.9: Recorded seismograms for several transmission experiments at $L = 424m$. The standard deviation in the left column is $\sigma = 4\%$ and in the right $\sigma = 8\%$. From top to bottom the correlation lengths are $a = 10, 40, 160m$. The dominant wavelength is in all experiments $\lambda \approx 40m$. The influence of σ and the interplay between λ and a can be clearly observed.

2.3 Statistics of randomly scattered wave fields

In seismology it is usual to analyze the wave field fluctuations and to relate them to statistics of the random medium heterogeneities. Usually the second statistical moments are computed (Wu and Flatté, 1990). Alternatively, we look for the probability density functions of the wave field fluctuations.

2.3.1 Analysis of amplitude and phase fluctuations

To characterize statistically the amplitude and phase fluctuations it is expedient to construct their probability density functions (PDF). First let us consider theoretically which PDF come into play. In the case of weak scattering we can describe wave fields in random media by the approach of Rytov. Hence, we assume that the distortion of the wave field u due to the presence of inhomogeneities is described by the complex exponent Ψ so that

$$u \propto e^{\Psi} = e^{\chi + i\phi} . \tag{2.48}$$

The real functions χ and ϕ are called log-amplitude and phase fluctuations, respectively. In appendix A.1 it is shown that by virtue of the (first) Rytov approximation the functions χ, ϕ can be represented as integrals over the fluctuating medium parameter. In a simplified picture one can think about it as a sum, where the contributions to χ and ϕ come from different depths intervals. If these intervals are larger than the characteristic size of the heterogeneities, these contributions are uncorrelated. Therefore, χ and ϕ can be thought of as sums of independent random variables. The central limit theorem states that a sum of N random variables assume normal (Gaussian) distribution if N is large enough, no matter what the PDF of individual random variables are. Then it is clear that χ and ϕ are normal distributed:

$$p(\chi) = \frac{1}{\sqrt{2\pi}\sigma} e^{-\frac{(\chi - m)^2}{2\sigma^2}} \tag{2.49}$$

with the parameters m and σ. According to the transformation law of random variables (Papoulis, 1984, pp. 93), measured amplitudes $A \propto e^{\chi}$ are lognormal distributed

$$p(A) = \frac{1}{\sqrt{2\pi}\sigma A} e^{-\frac{(\ln(A) - \eta)^2}{2\sigma^2}} \tag{2.50}$$

with the parameters η and σ.

A similar consideration of PDF's can be done for the case of strong scattering. Following Ishimaru (1978) we assume that the wave field scattered on a single scatterer can be represented as $u^1_{scatter} = Ae^{i\phi}$. The wave field due to many scatterers N is the superposition $u^N_{scatter} = \sum_{n=1}^{N} A_n e^{i\phi_n} = \sum_{n=1}^{N} X_n + iY_n$, where $X = A\cos(\phi)$ and $Y = A\sin(\phi)$. Since the scatterers are randomly distributed we have a sum of N independent random variables that assume the normal distribution due to the central limit theorem. Within the strong wave field fluctuation regime we assume also that the phase is uniformly distributed over 2π and that the joint probability density is given by $p(A, \phi) = p(A)p(\phi)$. Then, it is clear that $\langle X \rangle = \langle Y \rangle = \langle XY \rangle = 0$. But uncorrelated and normal random variables are independent (Hohnerkamp, 1990) so that $p(X, Y) = p(X)p(Y)$. Using these relations we obtain

$$\begin{aligned} p(A, \phi)\, dA d\phi &= p(X, Y) dX dY \\ &= \frac{1}{2\pi\sigma^2} e^{-\frac{X^2 + Y^2}{2\sigma^2}} dX dY . \end{aligned} \tag{2.51}$$

Re-substituting $X = A\cos(\phi)$ and $Y = A\sin(\phi)$ and noting that $dXdY = A\,dAd\phi$ one obtains from equation (2.51) after integrating with respect to ϕ

$$p(A) = \frac{A}{\sigma^2} e^{-\frac{A^2}{2\sigma^2}} \tag{2.52}$$

which is known as the Rayleigh distribution. To the above calculation it should be noted that whereas amplitudes and phases are statistically independent, the spatial variations of amplitude and phase at a certain point show correlations (Freund and Shvartsman, 1995).

From experiments it is difficult to distinguish between the lognormal and the Rayleigh distribution. Physically this expresses the fact that the transition from weak to strong scattering is smooth. We assume that throughout our numerical experiments the PDF of recorded amplitudes can be well approximated by the lognormal distribution. The simplest way to estimate the PDF in a numerical way is to construct the histograms. This is shown in the Figures (2.10) and (2.11), where the probabilities of recording a certain time (amplitude) interval are displayed as a function of the travel-distance. A more quantitative method is the maximum-likelihood method which we briefly outline in the following. The task is to determine the parameters of the lognormal distribution (σ, η) in equation (2.50). If for example in the plane wave experiment at a certain travel-distance N amplitude values A_i are measured, then the likelihood function is defined as

$$\begin{aligned} L(A_1..A_N, \eta, \sigma^2) &= \frac{1}{A_1\sqrt{2\pi}\sigma} e^{-\frac{(\ln(A_1)-\eta)^2}{2\sigma^2}} \cdot \frac{1}{A_2\sqrt{2\pi}\sigma} e^{-\frac{(\ln(A_2)-\eta)^2}{2\sigma^2}} \cdot .. \\ &= \left[\frac{1}{\sqrt{2\pi}\sigma}\right]^N \cdot \prod_i^N \frac{1}{A_i} \cdot e^{-\frac{1}{2\sigma^2}\sum_{i=1}^N (\ln(A_i)-\eta)^2}. \end{aligned} \tag{2.53}$$

The method consists in maximizing $\ln(L)$ for the parameters (σ, η). In other words, a maximum likelihood estimator of (σ, η) is determined by the system of equations

$$\begin{aligned} \frac{\partial \ln(L)}{\partial \eta} &= 0 \\ \frac{\partial \ln(L)}{\partial(\sigma^2)} &= 0\,. \end{aligned} \tag{2.54}$$

Substituting (2.53) into (2.54) we find

$$\sum_{i=1}^N \ln(A_i) - \eta = 0 \tag{2.55}$$

$$-\frac{N}{2}\frac{1}{\sigma^2} + \frac{1}{2\sigma^4}\sum_{i=1}^N (\ln(A_i)-\eta)^2 = 0\,. \tag{2.56}$$

From equation (2.55) one immediately finds $\eta = \frac{1}{N}\sum_{i=1}^N \ln(A_i)$ and equation (2.56) leads to $\sigma^2 = \frac{1}{N}\sum_{i=1}^N (\ln(A_i)-\eta)^2$. Lognormal PDF's for the amplitudes with numerically determined (σ, η) values are shown in Figure (2.11).

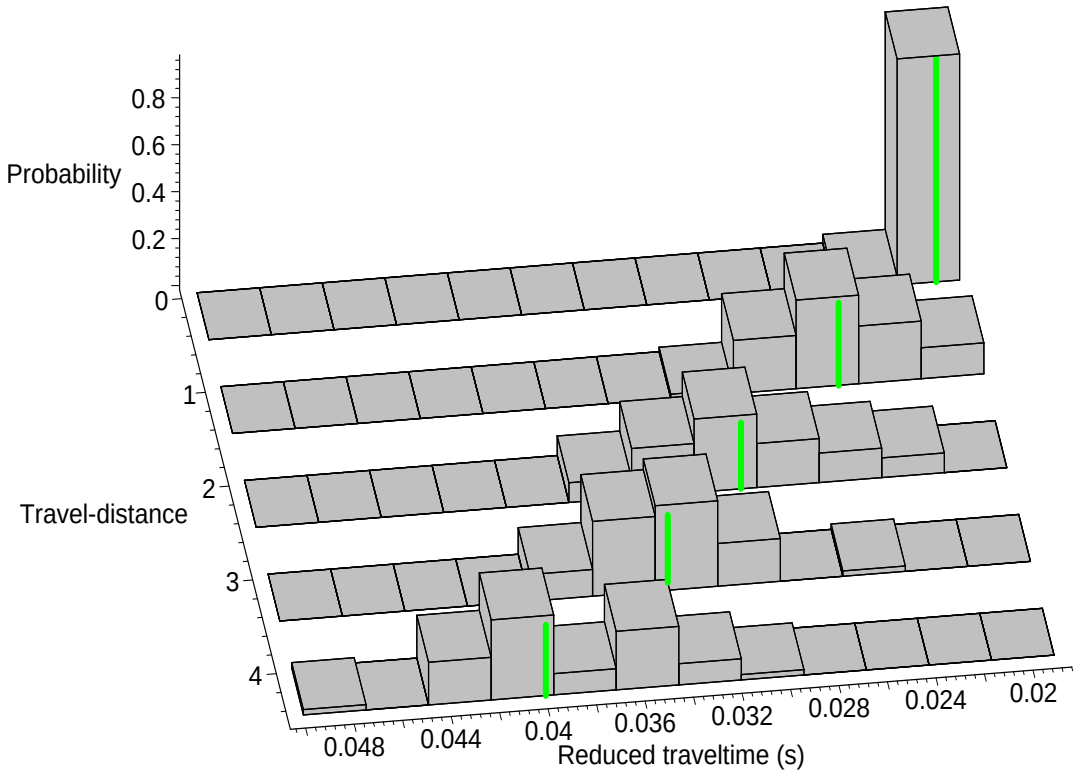

Figure 2.10: Probability of traveltimes of the primary wave field in the random medium as a function of travel-distance. The medium parameters are defined in section 2.2.2.

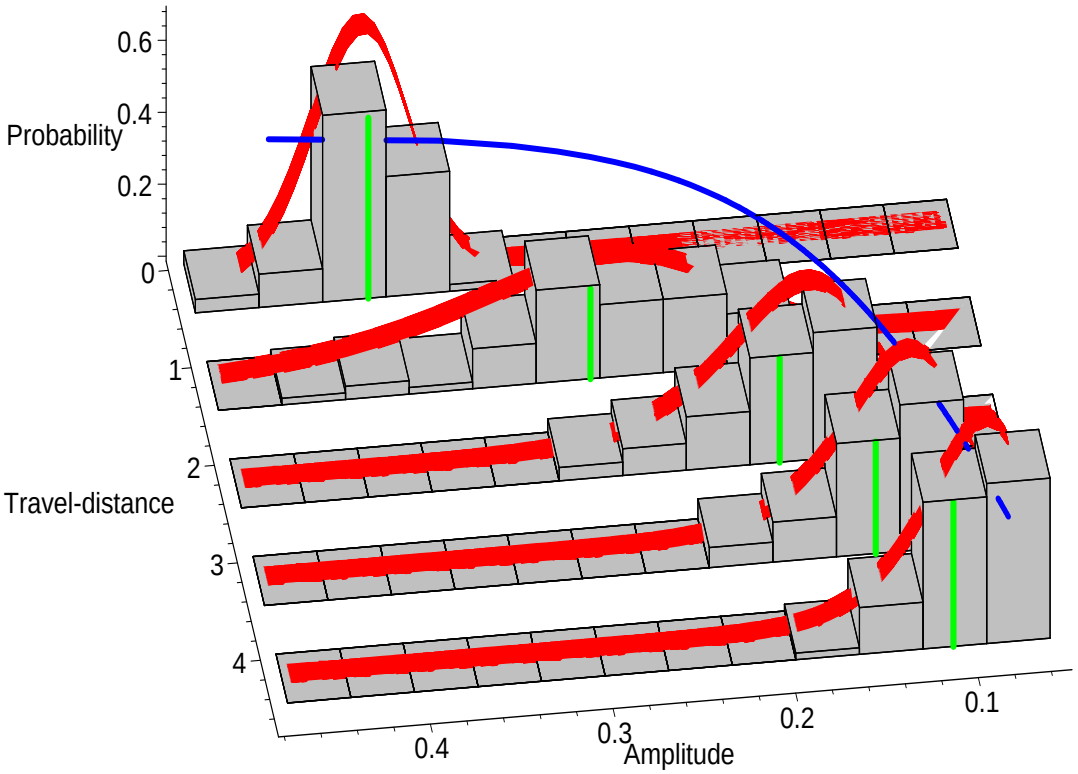

Figure 2.11: Probability of amplitudes of the primary wave field as a function of travel-distance. The red strips denote the PDF's determined by the maximum-likelihood method. The green vertical lines and the space curve through the maxima of the histograms result from an analytical approximation developed in chapter 3.

From Figures (2.10) and (2.11) it is obvious that the PDF are functions of the travel-distance and therefore of the traveltime. That is to say the PDF of amplitudes and phases evolve in time. Note that it is equivalent to study the wave propagation based on wave equations with random variables (i.e. stochastic differential equations) or solving the corresponding differential equations for the probability densities. The latter are known as the Fokker-Planck equations. In appendix A we show that within the Rytov approximation $\langle\chi\rangle = -\sigma^2_{\chi\chi}$ and the PDF (2.49) is then

$$p(\chi) = \frac{1}{\sqrt{2\pi}\sigma_{\chi\chi}}\, e^{-\frac{(\chi+\sigma^2_{\chi\chi})^2}{2\sigma^2_{\chi\chi}}}\,. \tag{2.57}$$

It is easy to verify that equation (2.57) is a solution of the Fokker-Planck equation

$$\frac{\partial}{\partial(\sigma^2_{\chi\chi})}\, p(\chi,\sigma^2_{\chi\chi}) = -\frac{\partial}{\partial\chi}\, p(\chi,\sigma^2_{\chi\chi}) + \frac{1}{2}\frac{\partial^2}{\partial\chi^2}\, p(\chi,\sigma^2_{\chi\chi}) \tag{2.58}$$

describing the so-called Ornstein-Uhlenbeck process (Gardiner, 1990).

2.3.2 Random focusing

Constructive interference of scattered waves lead to the effect of random focusing. That means, apart from the normal level of amplitude fluctuations, large amplitude fluctuations at randomly distributed spatial positions can be observed. This is shown in Figure (2.12), where 3 focal points can be identified (indicated by the arrows). The same effect can be also observed in the wave field snapshots in Figure (2.8). Note that these large amplitude fluctuations are not caused by large medium parameter fluctuations at the spatial positions of the focal points and that the random focusing is observed already within the weak wave field fluctuation regime. In the light of geometrical optics, such focal points correspond to caustics, where the amplitude tends to become infinite.

Within the framework of geometrical optics, Kulkarny and White (1982) statistically analyzed the random spatial distribution of caustics in 2-D random media. By solving the Fokker-Planck equations associated with the equations for the ray tube area and the wave-front curvature, they obtained the PDF for the (normalized) travel-distance $\tilde{L} = L/a$ to the first focus

$$p(\tilde{L}) = \left(\frac{K^2(1/2)}{\sqrt{2\pi}}\tilde{L}^{-5/2} + 0.314\right) e^{-\frac{K^4(1/2)}{6}\tilde{L}^3 - 0.281\tilde{L}}\,, \tag{2.59}$$

where K denotes the complete elliptic integral of the first kind. The constants 0.281 and 0.314 are universal. Its maximum is reached for

$$a\left(\int_{-\infty}^{\infty} dr\, \frac{d^4B(r)}{dr^4}\right)^{-1/3} \tag{2.60}$$

involving the fourth derivative of the medium correlation function and corresponds to a normalized travel-distance $\tilde{L} \approx 1.3$. (e.g., inserting the Gaussian correlation function in equation (2.60) yields $1.28\,a$). Equation (2.59) together with the inverted probabilities from the numerical experiment is shown in Figure (2.13).

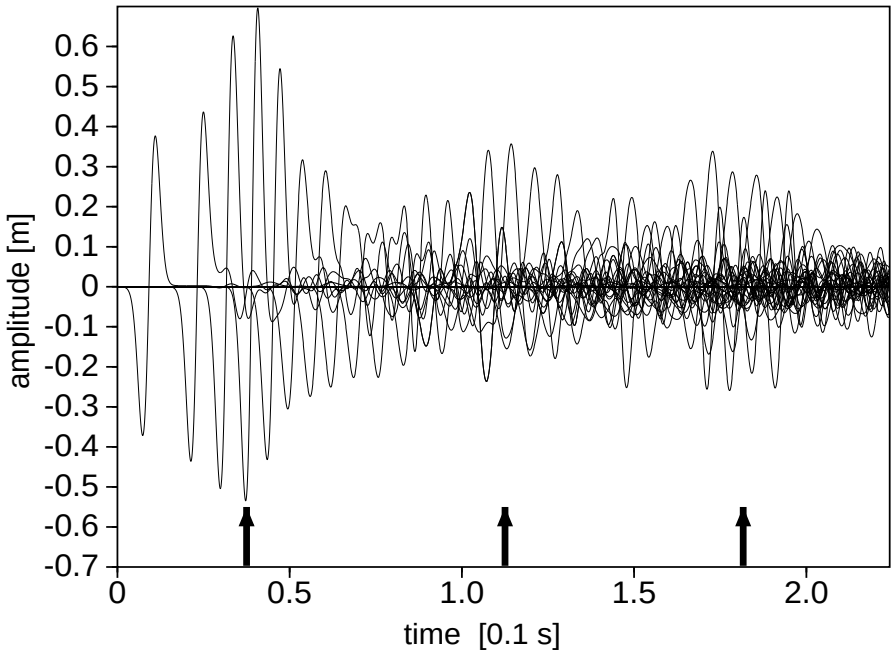

Figure 2.12: 40 traces recorded at 40 different depths (and the same transversal distance) inside the random medium (Gaussian correlated, $a = 45$, $\sigma_n = 0.15$). The numerical experiment is described in section 2.2.2. We observe the random focusing of the wave field. According to Kulkarny and White (1982) the focal distance is $\approx 1.3a$.

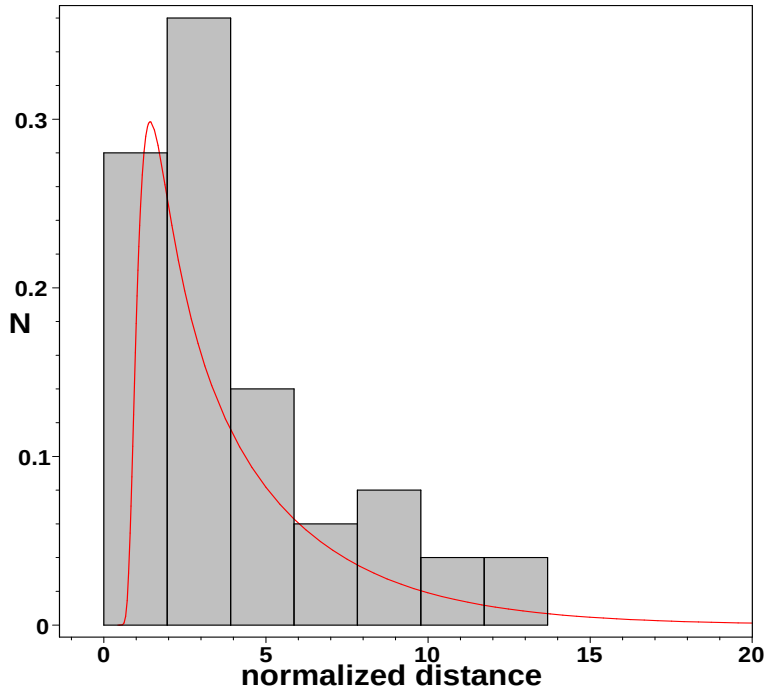

Figure 2.13: Probability density function for the random focusing distance (red line). The histogram depicts the focusing distances obtained from the numerical experiment described in section 2.2.2.